Plate coupling along the Manila subduction zone between Taiwan and northern Luzon

Article *in* Journal of Asian Earth Sciences · June 2012

DOI: 10.1016/j.jseaes.2012.01.005

4 authors, including:

Ya-Ju Hsu
Academia Sinica
63 PUBLICATIONS **1,278** CITATIONS

SEE PROFILE

Teh-Ru Alex Song
University College London
46 PUBLICATIONS **1,562** CITATIONS

SEE PROFILE

Journal of Asian Earth Sciences 51 (2012) 98–108

Contents lists available at SciVerse ScienceDirect

Journal of Asian Earth Sciences

journal homepage: www.elsevier.com/locate/jseaes

Plate coupling along the Manila subduction zone between Taiwan and northern Luzon

Ya-Ju Hsu [a,*], Shui-Beih Yu [a], Teh-Ru Alex Song [b], Teresito Bacolcol [c]

[a] Institute of Earth Sciences, Academia Sinica, Taipei, Taiwan
[b] Yokohama Institute for Earth Science, Institute for Research on Earth Evolution, Japan Agency for Marine-Earth Science and Technology, Yokohama, Japan
[c] Philippine Institute of Volcanology and Seismology, Quezon City, Philippines

ARTICLE INFO

Article history:
Received 16 March 2011
Received in revised form 5 January 2012
Accepted 20 January 2012
Available online 1 March 2012

Keywords:
Manila subduction zone
Plate coupling
Backslip
Dislocation model

ABSTRACT

We use GPS data, trench parallel gravity anomaly (TPGA), and bathymetry to infer plate coupling patterns along the Manila subduction zone. Using a block model and a fault geometry constrained by seismicity, we simultaneously solve for the location of Euler pole and angular velocity between the Sunda and Luzon blocks as well as the slip-deficit rate on plate interface. Our estimates show that the Euler pole between the Sunda and Luzon blocks is situated at southern Palawan near 8.3°N and 119.4°E with the angular velocity of 4.6 Myr^{-1}. The estimated convergence rate along the Manila Trench continuously decreases southward from 91 mm/yr at the northern tip of Luzon to 55 mm/yr north of Mindoro. The inversion of GPS data reveals partially locked fault patches extending from the West Luzon Trough to the east of Scarborough Seamount chain. The slip-deficit rate in this region is in the range of 20–30 mm/yr corresponding to a coupling ratio of 0.4. However, the fault slip behavior is not well resolved near the North Luzon Trough. Based on a good correlation between locations of large subduction zone earthquakes and areas possessing gravity low, we investigate a variety of TPGA-based plate coupling models assuming different scaling between TPGA values and plate coupling ratios. The TPGA-based plate coupling models offer plausible rupture scenarios which are not constrained by current GPS data. The partially locked fault zone near 15–16.5°N may be associated with the subducted Scarborough Seamount wherein oceanic floor is highly fractured. The great subduction zone earthquake propagates beneath the Scarborough Seamount seems to be unlikely. The densification of GPS network in central Luzon and seafloor geodetic observations close to trench axis are crucial to distinguish the detailed fault coupling patterns and the role of subducted seamounts.

1. Introduction

The most devastating earthquakes and tsunamis in the world occur in subduction zones. However, the seismogenic behaviors of many subduction zones remain poorly understood owing to the limited spatial coverage of seismic and geodetic data. The Manila subduction zone located at the plate boundary wherein the Philippine Sea Plate converges obliquely toward the Sunda Plate/Eurasian Plate with a rate of 80–100 mm/yr in the region between offshore southern Taiwan to northern Luzon of Philippines (Seno et al., 1993; Yu et al., 1999; Sella et al., 2002). Recent data derived from GPS (Rangin et al., 1999; Simons et al., 1999; Kreemer et al., 2000; Bacolcol et al., 2005) and earthquake slip vectors (Chamot-Rrooke and Le Pichon, 1999) showed that the Sunda Plate is a distinct entity and rotates clockwise with respect to the Eurasian plate (Chamot-Rrooke and Le Pichon, 1999). The convergence rate between the Sunda Plate and Philippine Sea Plate tapers gradually towards to the south as collision tectonic pins on the southern end of the Manila subduction zone (Rangin et al., 1999). The oblique convergence is partitioned into a 40–90 mm/yr trench normal component on the subduction thrust and a ~25 mm/yr component of sinistral slip along the Philippine fault (Fig. 1a–b) (Barrier et al., 1991; Aurelio, 2000; Megawati et al., 2009; Yu et al., 2011). Convergence also exists to the east of Luzon along the East Luzon Trough but it is insignificant as this trough is nearly entirely shifted by the arrival of the Benham plateau (Karig, 1983; Lewis and Hayes, 1984). To the south of Luzon, the convergence flips to the eastern side of Luzon and transfers to westward subduction along the Philippine Trench (Fig. 1b).

Historic records indicate large tsunamis have hit the China coast and western Luzon in the past three centuries (Wang and Zhang, 2005; Megawati et al., 2009). The two most suspicious events which could have been occurred on the Manila subduction zone

* Corresponding author. Address: Institute of Earth Sciences, Academia Sinica, P.O. Box 1-55, Nankang, Taipei 115, Taiwan. Tel.: +886 2 2783 9910x416; fax: +886 2 2783 9871.
E-mail address: yaru@earth.sinica.edu.tw (Y.-J. Hsu).

1367-9120/$ - see front matter © 2012 Elsevier Ltd. All rights reserved.
doi:10.1016/j.jseaes.2012.01.005

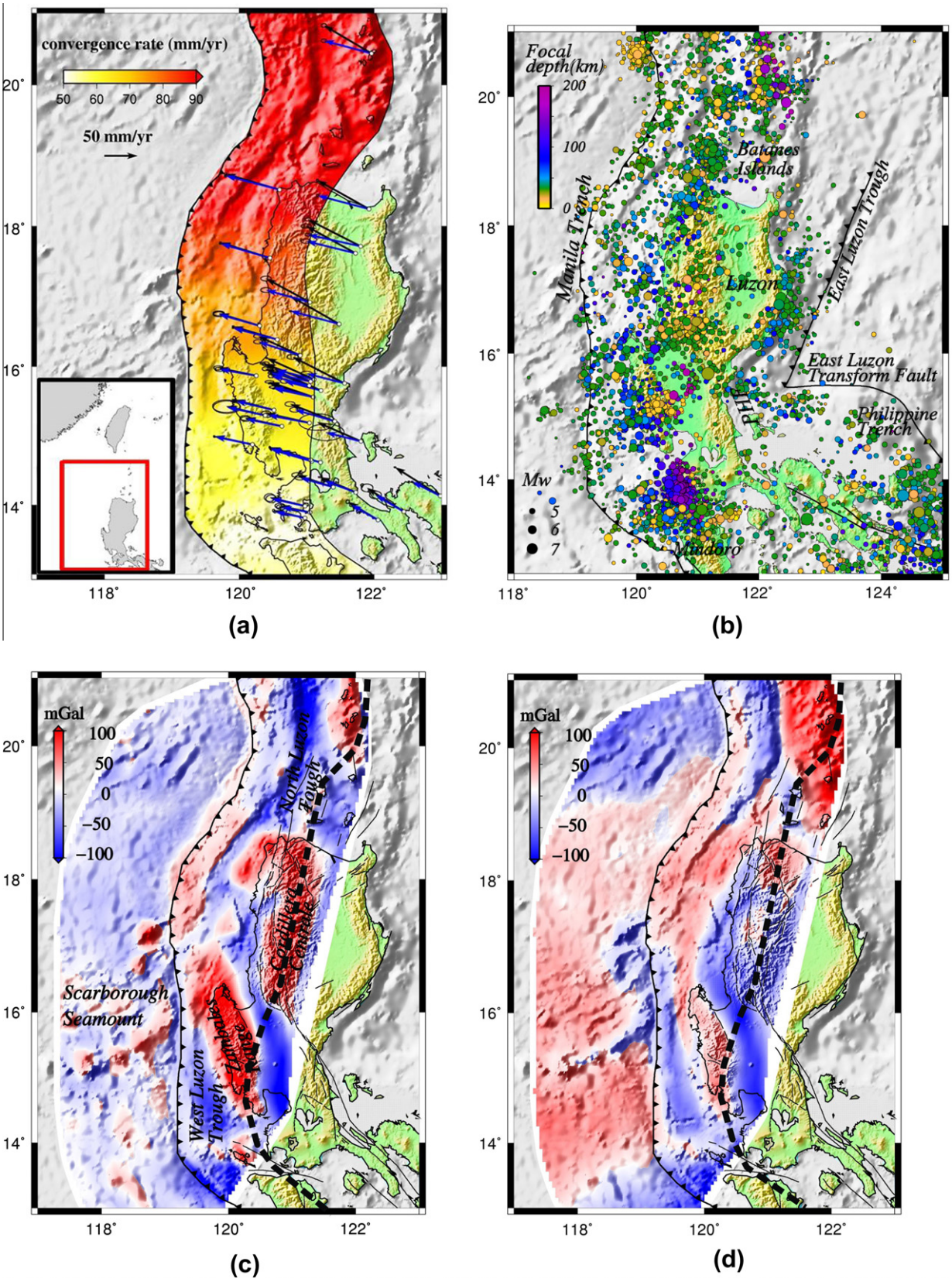

Fig. 1. Plate boundary deformation and trench parallel gravity anomaly along the Manila subduction zone. (a) Black vectors are GPS station velocities in the Sunda fixed reference frame. Error ellipses indicate 95% confidence intervals of GPS velocities. Blue vectors are velocities corrected for fault locking effect on the Philippine Fault (PHF in (b)). The yellow–red color scale indicates plate convergence rate. Bathymetry is shown in grey scale. The inset shows the regional geography with a red box indicating the study area (b) The seismicity is in the time period between 1973 and 2010 from NEIC (the US Geological Survey National Earthquake Information Center). The moment magnitude is in the range between 4.6 and 7.7. Color scale indicates focal depth. (c) The shaded relief topography and estimated free-air TPGA on the Manila subduction zone (Sandwell and Smith, 2009). The color bar indicates the amplitude of TPGA values. The black barbed and dashed lines denote the Manila Trench and 50 km slab iso-depth, respectively. (d) The Bouguer TPGA at the Manila subduction zone.

are the 1076 and 1781 events (Megawati et al., 2009). However, no large earthquakes with moment magnitude (M_w) larger than 8 have been observed since the Spanish colonization of Luzon in the 1560s. The seismicity between 1973 and 2010 also indicates that large earthquakes ($M_w \sim 7$) are not very frequent on the Manila subduction zone (Fig. 1b). A paucity of large earthquakes may imply either a predominately aseismic subduction along the Manila Trench or a seismically active subduction in a stage of quiescence period before giant earthquakes. If the characteristics of Manila subduction zone fall into the second case, the seismogenic behavior could be similar to the Sunda–Andaman subduction zone before the occurrence of the 2004 M_w 9.3 Aceh–Andaman earthquake (Chlieh et al., 2007). No great earthquakes ($M_w > 8$) is known to have occurred between Sumatra and Myanmar in the historic record. Modeling from the tsunami record only reveals large earthquakes with magnitudes between 7.5 and 7.9 (Ortiz and Bilham, 2003; Bilham et al., 2005). The $M_w \sim 9$ giant earthquakes had never been anticipated for the Sunda–Andaman subduction zone before the 2004 earthquake. It appears that our knowledge of seismogenic process of giant subduction earthquakes is insufficient at present. Since a large population live in coastal areas of the South China Sea, it is important to examine the possibility of giant earthquakes on the Manila subduction zone.

Previous studies have shown some parameters varying along the trench may influence seismogenic behaviors and mechanical properties on the plate interface. Important parameters include the age of subducting seafloor, plate convergence rate (Ruff and Kanamori, 1980; Kanamori, 1986), sediments (Ruff, 1989), and back-arc spreading (Uyeda and Kanamori, 1979). The great earthquakes tend to occur in subduction zones with faster convergence, younger lithosphere, and excess trench sediments; while the relative aseismic subduction zones are characterized by slower convergence and older lithosphere. In the Manila subduction zone, the age of subducting seafloor decreases from 32 Ma offshore northern Luzon to about 17 Ma near the Scarborough Seamount (part of an extinct mid-oceanic ridge, Fig. 1) (Hayes and Lewis, 1984). A similar trend of a southward decrease of plate convergence rate from 85 mm/yr at Batanes to 49 mm/yr north of Mindoro is also observed from GPS data (Fig. 1a and Yu et al. (2011)). The Manila trench sediments can be divided into two sections; a sediment-filled section (~5 km thick) that extends from offshore SW Taiwan to 16.5°N wherein the Scarborough Seamount is being subducted and a sediment-free section from 16.5°N to Mindoro (Ludwig et al., 1979). Additionally, no active back-arc spreading is shown on the overriding Philippine Sea Plate suggesting that the plate motion is seismic. These features are similar to the Sumatra–Andaman subduction zone wherein the age of seafloor and the sediment thickness decrease southward (Chlieh et al., 2007), whereas the plate convergence rate on the Sumatra–Andaman subduction zone increases southward, opposite to that at the Manila subduction zone. More recent studies have shown no significant correlations between these subduction zone parameters (Pacheco et al., 1993). The observed variations in plate coupling may be attributed to the subduction of bathymetric features (Cloos, 1992; Scholz and Small, 1997; Bilek et al., 2003), mechanical and material properties of subducted sediments (Hyndman et al., 1997; Peacock and Hyndman, 1999), and some other factors (Stern, 2002). Understanding these variations is crucial to evaluate seismic hazards at subduction zones.

This study aims to give a better estimation of plausible rupture sources along the Manila Trench using GPS data. We also explore possible plate coupling models using the trench-parallel gravity anomaly (TPGA) and bathymetry (Fig. 1). The GPS velocity measurements allow for direct estimation of the degree of plate coupling during the time period of observation (Savage, 1983). However, plate coupling ratio is not well constrained by GPS data alone due to the limited spatial coverage of GPS sites close to the trench axis (Fig. 1a). Previous studies have documented that great subduction earthquakes occur predominately on the plate interface beneath forearc basins (Song and Simons, 2003; Wells et al., 2003) and in areas possessing a strongly negative TPGA, whereas regions with strongly positive TPGA are relatively aseismic (Song and Simons, 2003). The study on the relationship between the spatial extent of great subduction earthquakes and the TPGA also show an increase in TPGA between the earthquake centroid and the limits of the rupture (Llenos and McGuire, 2007). Based on a good correlation between areas possessing negative TPGA, forearc basins, and the locations of megathrust rupture zones, we develop a variety of models assuming different scaling between plate coupling ratio and TPGA values. We then compute surface velocities at GPS sites from this model and compare them with GPS observations. This approach allows us to explore if locked asperities defined by strongly negative TPGA are able to reproduce geodetic measurements and provide some plausible coupling patterns for the Manila subduction zone. Additionally, we test three uniform plate coupling models with various coupling ratio as well as forward models with coupling ratios exhibiting a Gaussian decay function on the fault zone. Our work provides several candidates of plate coupling models with satisfactory fits to GPS observations. The predicted velocity variations from these models would benefit future GPS site selection in Luzon and further clarify the validity of present models.

2. Data

2.1. GPS

The campaign-mode GPS network in Luzon was established in late 1995 and first measured in 1996 by the Institute of Earth Sciences, Academia Sinica, Taiwan in collaboration with the Philippine Institute of Volcanology and Seismology, Philippines (Yu et al., 1999). The network was initially composed of 15 stations and additional 16 stations were added into the network in central and southern Luzon between 1998 and 1999. Succeeding GPS surveys were done annually until 2000. Three more campaigns were conducted in 2004, 2006, and 2008, respectively (Yu et al., 2011). For each campaign, most sites were observed continuously for 2–3 days using dual-frequency, geodetic GPS receivers, in a 30-s sampling rate.

The collected GPS data are processed with GAMIT/GLOBK software packages, version 10.3 (Herring et al., 2002) using the double-difference phase observable and tropospheric and ionospheric modeling. To obtain a more accurate and consistent regional deformation pattern of the Luzon Island, we use GPS data from 30 Luzon sites, 17 permanent IGS sites in the Asia–Pacific region, and six sites from Taiwan continuous GPS Array in southern Taiwan. Fourteen IGS sites with long observation history surrounding the study area are constrained to their 2005 International Terrestrial Reference Frame (ITRF2005, Altamimi et al., 2007) coordinates in GLOBK processing, together with the parameters from GAMIT solutions to produce ITRF2005 coordinates of other GPS sites. A least squares linear fit is used to estimate station velocity from station position time series. The ITRF2005 velocities are transformed into the Sunda fixed reference frame (Yu et al., 2011). The station velocities with respect to the Sunda Plate are about 49–85 mm/yr, in the west-northwest (WNW) to northwest (NW) directions and gradually decrease from north to south (Fig. 1a).

2.2. Bathymetry

The Sunda Plate subducts beneath the Philippine Sea Plate along the 5 km-deep Manila Trench. The trench is N–S trending from

14°N to 18°N and bends to NE trending to the north of 18°N and SE trending to the south of 14°N (Fig. 1). The subduction process is replaced by collision tectonics on the northern tip of the Manila Trench near Taiwan (Bowin et al., 1978; Page and Suppe, 1981) and on the southern tip of the trench between Palawan and Mindoro (Rangin et al., 1999). On the eastern side of the Manila Trench, there are two major forearc basins called the North Luzon Trough from 18°N to 21°N and the West Luzon Trough from 14°N to 16°N (Fig. 1c). The sediment thickness in troughs can be up to 4–5 km thick (Ludwig, 1970; Hayes and Lewis, 1984). The Scarborough Seamount chain, a bathymetric high, can be traced from 115°E to 119°E at 16°N (Fig. 1c), and it is related to the subduction of a NE trending extinct ocean ridge of the South China Sea spreading center on the western side of the Manila Trench. These seamounts have being subducted obliquely along the Manila Trench (Pautot and Rangin, 1989).

2.3. Gravity

We construct TPGAs near the Manila subduction zone using global marine gravity grids (Sandwell and Smith, 2009) and the method proposed by Song and Simons (2003). An average regional trench-normal gravity profile was subtracted from the original free-air gravity (Sandwell and Smith, 2009) because that the trench-normal gravity is predominantly controlled by mantle rheology, slab buoyancy, and stress conditions on the plate. In this study, we only consider TPGA values over the location of the plate interface where megathrust earthquakes occur (less than 50 km depth). The resulting TPGA for the Manila subduction zone is shown in Fig. 1c. Two forearc basins, North Luzon Through and West Luzon Trough, are characterized by strongly negative TPGA values of about −100 and −50 mGal, respectively. The Cordillera Centrale and the Zambales Range show positive TPGA values of about 50–100 mGal. The north–south trending Cordillera Centrale is composed of plutonic rocks and is part of the volcanic arc related to the subduction at the Manila Trench. The Zambales Range consists of ophiolite assemblage and represents uplifted crust associated with both oceanic basin and island arc affinities (Hayes and Lewis, 1984). To investigate the influence of seamount or aseismic ridge on plate coupling, we also construct TPGA using the Bouguer gravity anomalies based on the assumption of local compensation (Fig. 1d). The negative Bouguer anomalies usually correlate with sedimentary basins, the roots of mountains, seamounts, or ridges. The TPGA values constructed from Bouguer anomalies are less negative in the two forearc basins and less positive in the Cordillera Centrale and the Zambales Range compared to those from free-air anomalies (Fig. 1c–d). Note that the gravity data near the Zambales Range are relative sparse.

3. Method

We construct the slab geometry based on earthquake focal mechanisms in the time period between 1973 and 2010 from NEIC (the US Geological Survey National Earthquake Information Center) and the curvature of Manila Trench (Fig. 2). The trench normal cross sections of seismicity indicate that the slab dips eastward to about 10–20° at shallow depths and steepens to around 30° at depths greater than 30 km in offshore northern Luzon. The slab dip steepens in the Luzon area, as shown in focal depths and high-angle thrust faulting mechanisms. The slab changes dip from 30° to 50° at a depth of 50 km at latitude 15°N. Our model fault approximately follows the curvature of the 5-km deep trench and has a dimension of 1100 km in length and 230 km in width (Fig. 2). The fault geometry is consistent with the 3D geometry of the plate interface delineated from seismicity and focal mechanisms based on first motion solutions and Global CMT solutions (Bautista et al., 2001). We divided the fault into 104 patches with 26 and 4 patches in the along-strike and down-dip directions, respectively. The patch size is about 45 km by 45 km and the Green's function of each fault patch is calculated using an elastic half-space model (Okada, 1985).

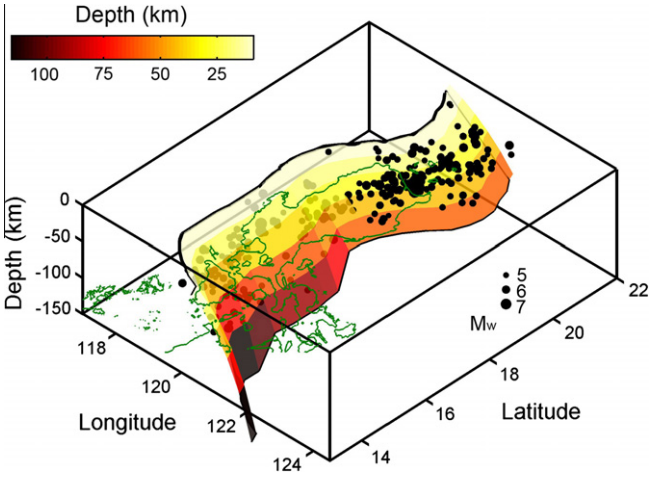

Fig. 2. The fault geometry of the Manila subduction zone. Color scale indicates the depth of the fault plane. Black dots denote the seismicity is in the time period between 1973 and 2010 from NEIC. The fault dip steepens from north to south.

The effect of interseismic strain accumulation can be represented as the sum of the long-term block motion across the plate boundary fault and slip on the locked fault zone (Savage, 1983). Here we use a similar approach but for a three-dimensional elastic block that interseismic GPS velocities can be decomposed into a rigid block rotation and fault slip at block boundaries. To define block boundaries, we first examine early studies of plate models based on geological, geomagnetic, and geodetic data (Seno et al., 1993; Sella et al., 2002; Kreemer et al., 2003). We compute plate convergence rate between the Philippine Sea Plate and the Sunda Block using these models and find that the convergence rate falls in the range of 80–100 mm/yr between Taiwan and Luzon and increases southward. However, GPS velocities indicate a southward decrease from northern to southern Luzon, disagrees with rates predicted by aforementioned plate models. We then consider Luzon as an elastic block as proposed in Rangin et al. (1999), except for areas near the Philippine fault. Rangin et al. (1999) shows that the convergence rate between the Luzon and the Sunda blocks decrease from 100 mm/yr at northwestern tip of Luzon to a rate of 50 mm/yr near the latitude of 15°N at southern Luzon.

In this study, we do not consider the motion of the Luzon block with respect to the Philippine Sea Plate, which is mainly accommodated by the East Luzon Trough, East Luzon Transform fault, and the northern part of the Philippine Trench (Fig. 1b). The westward subduction along the East Luzon Trough may have ceased as indicated on seismic profiles (Lewis and Hayes, 1984). Only a small amount of E–W convergence was seen to its southern extremity. Since most of convergence at the latitude of Luzon is absorbed along the Manila Trench (Rangin et al., 1999) and our GPS sites in eastern Luzon are located about 100 and 250 km to the west of the East Luzon Trough and the Philippine Trench, respectively, presumably have a little effect from the westward subduction of the Philippine Sea Plate (Fig. 1b).

Here we consider the Luzon forms a relatively uniform block and determine its kinematics with respect to the Sunda block. We take the initial values of the Euler pole (9.3°N, 118.3°E, 5.5 Myr^{-1}) between the Luzon block (LU) and Sunda block (SU) from Rangin et al. (1999) and remove interseismic strain

accumulation along the Philippine fault from Yu et al. (2011). They show that the geodetic long-term slip rates on the Philippine fault increase from 24 mm/yr in northern Luzon to 40 mm/yr in southern Luzon. The inferred slip-deficit rate from GPS data is close to long-term slip rate suggesting that the Philippine fault is nearly fully locked. We subtract the interseismic fault locking effect on the Philippine fault from original GPS velocity field. Fig. 1a shows that the corrected GPS vectors are more perpendicular to the trench. After this correction, we simultaneously solve for the Euler pole location, the rotation rate of LU/SU, and the slip deficit rate at the Manila subduction zone.

We use a weighted least square approach to invert for the optimal slip deficit distribution which minimizing the weighted residual sum of squares (χ_r^2) and preserving some degree of smoothness in the model slip distribution. We impose the smoothness constraint on slip distribution using the finite difference approximation of the Laplacian (Harris and Segall, 1987). The damping parameter which characterizes the weight put on the model smoothness and data misfit, is determined by cross validation (Matthews and Segall, 1993). The fit to the data is quantified from the mean of the normalized square residuals. A value of 1 of χ_r^2 means that the model fits the data within uncertainties on average. The plate coupling ratio is given by the slip deficit rate divided by the block motion.

While we attempt to compute plate coupling ratio based on GPS data, finer details of slip on the megathrust is not resolved because of the scarcity of GPS sites near the Manila Trench. Song and Simons (2003) found a good correlation among negative free-air TPGA, topographic depression, and seismic moment. About 80% of the cumulative moment since 1900 has been released in 30% of total area of subduction zone with free-air TPGA less than −30 mGal. In this study, we construct TPGA both from free-air gravity and Bouguer gravity anomalies assuming that the plate coupling pattern resembles the distribution of TPGA such that the slip-deficit rate is linearly proportional to negative TPGA values. We also explore an inverse scaling between the free-air TPGA and plate coupling. In other words, positive free-air TPGA will correspond to strong coupling. Since the location of seamount is normally associated with positive free-air TPGA. The threshold used for the normalization of TPGA values is determined according to Song and Simons (2003). They divided the total area of subduction zone interface into four bins of approximately equal area. Areas with strongly negative TPGA (<−40 mGal) are fully locked (coupling ratio = 1) and with positive TPGA (>40 mGal) are creeping at plate convergence rate (coupling ratio = 0). The coupling ratios in the regions with TPGA values between −40 and 40 mGal are normalized to the range between 1 and 0. The slip-deficit rate is equivalent to the product of the normalized TPGA value and plate convergence rate. In order to find the best TPGA-based plate coupling model, we also apply different scaling between TPGA and slip-deficit rate. The predicted surface velocities from these models are used to compare with GPS velocities and provide plausible rupture scenarios based on TPGA-based plate coupling model. Additionally, we also test three uniform plate coupling models by assuming that the plate interface is fully-coupled, half-coupled, and decoupled and three models with coupling ratios exhibiting as a Gaussian decay function from the top, middle, and bottom of the fault plane. The model results are listed in Table 1, Figs. 3 and 4, and discussed in the following paragraph.

4. Results

The block model inverted from GPS data produces a χ_r^2 of 3.9 as shown in Fig. 3a. We determine the best Eulerian pole between LU and SU is situated in southern Palawan near 8.3°N and 119.4°E with the angular velocity of 4.6 Myr^{-1}. The estimated convergence rate along the Manila Trench continuously decreases from 91 mm/yr at the northern tip of Luzon to 55 mm/yr at 14°N (Fig. 3a). In the region near Northern Luzon Trough, the average slip-deficit rate is about 10 mm/yr (Fig. 3a), indicating a partially locked fault zone located to the west of the Batanes Islands. However, there is only one GPS site, BTS3, situated about 200 km away from the trench axis (Fig. 3b), the resolution of plate coupling near the North Luzon Trough is poor. To the south, a partially locked fault segment extends from latitude 15°N to 20°N. The area at latitudes 14.5–17°N from the West Luzon Trough to the east of Scarborough Seamount shows the slip-deficit rate in the range of 20–30 mm/yr with a predominately dip-slip motion. Given the plate convergence rate of 70 mm/yr, the coupling ratio is equivalent to 0.4. For the region south of 14°N, the plate coupling ratio is not well constrained due to the scarcity of GPS observations.

Limited by insufficient GPS data, we also explore different scenarios of interseismic slip-deficit rate along the Manila Trench. We consider five versions of scaling between TPGA and plate coupling ratio and assume that negative free-air TPGA is proportional to strong coupling (Table 1). The first model assumes a liner correlation between negative free-air TPGA and slip-deficit rate and produces a χ_r^2 of 14.1. In the rest models, we assume slip-deficit rates are proportional to square, cubic, square root, and cubic root of negative free-air TPGA values and compute the fits to GPS observations (Table 1). The values of χ_r^2 is close to 10 in the first two models; while the χ_r^2 values increase to 20 for the last two models. The slip-deficit model based on the cubit of free-air TPGA values gives the best fit with a χ_r^2 of 10.9. This model shows a strong coupling beneath the North Luzon Trough, the West Luzon Trough, and the downdip edge of the fault plane near 14°N and 16°N (Fig. 3d). Since the subducted Scarborough Seamount chain is a distinct feature at the Manila Trench, we used two approaches to demonstrate the influence of seamounts on plate coupling. We first assume that positive free-air TPGA is proportional to strong coupling. Thus the coupling pattern (Fig. 3e) is opposite to the previous model where the negative free-air TPGA is proportional to

Table 1
Elastic dislocation model results for a variety of plate coupling models. Bold texts show best models from different approaches.

Model	GPS inversion	Uniform coupling				TPGA-based plate coupling models, plate coupling ratio (c) $\propto$ (TPGA)^n				
Plate coupling	Spatial variable	Zero $c = 0$	Half $c = 0.5$	Fully $c = 1$		Linear ($n = 1$)	Square ($n = 2$)	Cubic ($n = 3$)	Square root ($n = 0.5$)	Cubic root ($n = 0.33$)
χ_r^2	**3.9**	**13.2**	15.4	61.4	$(FA)^{+n}$	14.1	11.5	**10.9**	18.8	21.8
					$(FA)^{-n}$	23.8	17.1	**14.4**	31.8	36.2
					$(BA)^{+n}$	12.9	10.9	**10.6**	17.5	20.9

χ_r^2: reduced chi-square.
c: plate coupling ratio, defined as the ratio of backslip rate to the plate convergence rate.
$(FA)^{+n}$: plate coupling ratio is proportional to negative free-air TPGA.
$(FA)^{-n}$: plate coupling ratio is inversely proportional to negative free-air TPGA, meaning strong coupling corresponding to positive free-air TPGA.
$(BA)^{+n}$: plate coupling ratio is proportional to negative Bouguer TPGA.

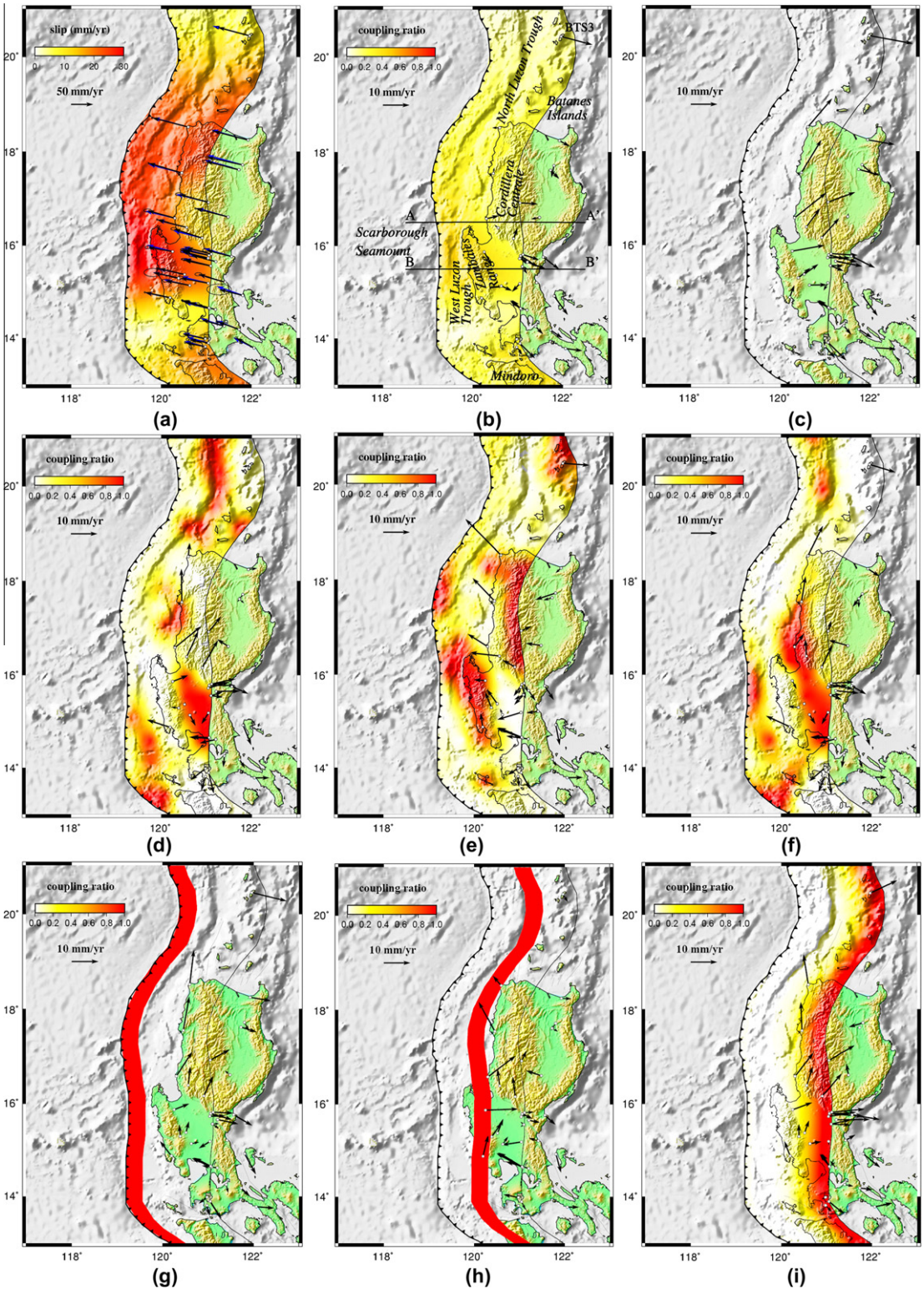

Fig. 3. Plate coupling models derived from GPS inversion, uniform coupling, and TPGA values. (a) Black and blue vectors indicate GPS observed and predicted interseismic velocities from inversion of GPS data. Error ellipses indicate 95% confidence intervals of GPS velocities. Color scales indicates fault slip rate. (b) Black vectors show residuals of horizontal velocities in (a). Color scale indicates coupling ratio. *A*–*A*′ and *B*–*B*′ show the locations of profile illustrated in Fig. 6 (c) GPS residuals computed from a zero coupling model. (d) The model with strong coupling proportional to the cubic of negative free-air TPGA. Black vectors are residuals of horizontal velocities. Color scale indicates coupling ratio. (e) The model with strong coupling proportional to the cubic of positive free-air TPGA. (f) The model with strong coupling proportional to the cubic of negative Bouguer TPGA. (g) The model with coupling ratio varies from 1 at trench axis to 0 at the bottom of the fault ($D = 30$ in Fig. 4a). (h) The coupling ratio varies from 1 in the middle of the fault to 0 at both sides of fault ($D = 30$ in Fig. 4b). (i) The coupling ratio varies from 0 at trench axis to 1 at the bottom of the fault ($D = 50$ in Fig. 4c).

strong coupling (Fig. 3d). A prominent asperity is shown beneath the Zambales Range. This model gives a χ_r^2 of 14.4 and provides a reasonable fit at latitudes 14–16°N (Figs. 3e and 6b). Secondly, we constructed TPGA using the Bouguer gravity anomalies because negative values usually correlate with roots of seamounts or ridges. The best plate coupling model obtained from the cubic of

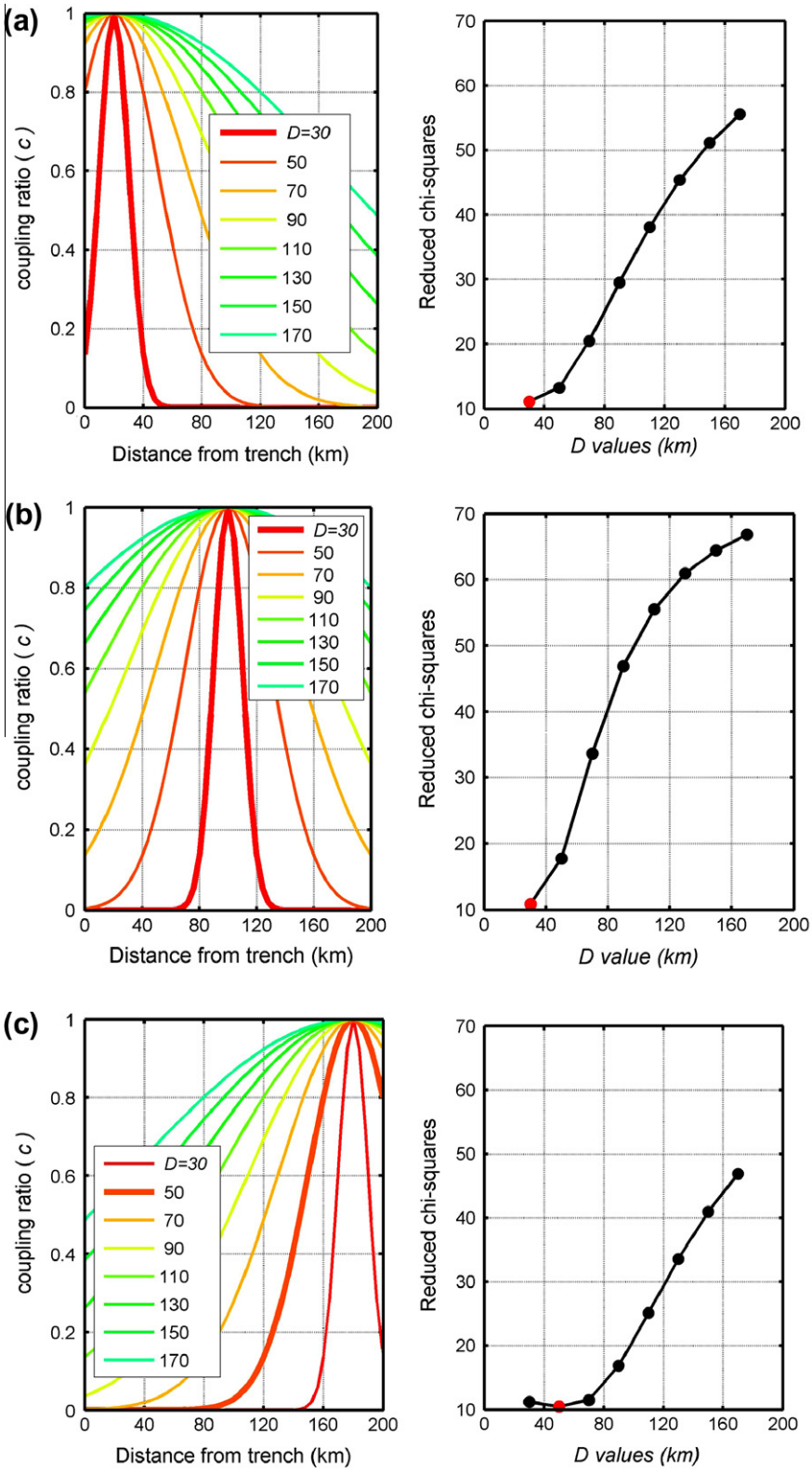

Fig. 4. Plate coupling models with coupling ratios vary as a Gaussian function. (a) The coupling ratio varies from 1 at trench axis to 0 at the bottom of the fault; (b) from 1 in the middle of the fault to 0 at both sides of fault; (c) from 0 at trench axis to 1 at the bottom of the fault. The color lines in left panels show a variety of coupling patterns from trench axis to the Luzon inland area. The optimal model with the smallest reduced chi-squares is shown in thick line. The right panel indicates the values of reduce chi-squares from all models given a wide range of the distance-decaying constant (D). The optimal model is shown as a red dot.

Bouguer TPGA shows locked patches near the trench at latitude 20°N, 15–16°N, and along the down-dip boundary of the fault near 14–18°N (Fig. 3f). This model results in a χ_r^2 of 10.6 and a satisfactory fit at latitudes 14–17°N (Figs. 3f and 6).

To find plausible rupture scenarios which are not constrained by GPS data, we also explore three uniform coupling models by assuming that the plate interface is fully-coupled, half-coupled, and decoupled and three models with coupling ratios exhibiting a Gaussian decay function from the top, middle, and bottom of the fault plane. The values of χ_r^2 from uniform coupling models are listed in Table 1. The decoupled and half-coupled plate models give similar values of χ_r^2 between 13 and 15, comparable with 10–14 obtained from the best TPGA-based plate coupling models (Table 1). The reduced-chi-square significantly increases to 61.4 for a fully-coupled model suggesting this scenario is not likely to happen at the Manila subduction zone. Fig. 4 shows the values of χ_r^2 from models with plate coupling ratios vary as a Gaussian function, $c = \exp(-d^2/D^2)$, where c is the coupling ratio, d is the distance, and D is the distance-decaying constant. The coupling ratio varies from 1 at trench axis to 0 in inland area (Fig. 4a), from 1 in the middle of the fault to 0 at both sides of the fault (Fig. 4b), from 0 at trench axis to 1 in inland area (Fig. 4c). The smallest value of χ_r^2 is ~10 in these three models, comparable to the decoupled and half-coupled plate models and the best TPGA-based coupling models (Table 1). The model with locked fault zone in the middle (Fig. 3h) provides a slightly better fit compared to others (Figs. 3g and i). These forward models suggest the plate interface is partially coupled; while the spatial extent of the locked area is not well resolved everywhere.

Fig. 3 shows a schematic of the comparison of plate coupling models based on different approaches. We examine residuals of GPS horizontal velocities and plate coupling patterns and evaluate seismogenic behaviors from north to south along the Manila subduction zone. Two plate coupling models at latitudes 19–21°N (Fig. 3d and h) provides satisfactory fits to the observed GPS velocity at BTS3 and suggests the possibility with locked fault patches beneath the North Luzon Trough is higher than the rest coupling models. At the NW corner of Luzon (17–19°N), the smaller residuals in Fig. 3b and d compared to others, suggest that fault is partially locked between the trench axis and the west Luzon coast; while the spatial extend is not well resolved. The GPS stations located between 14.5°N and 16.5° N are closest to the trench axis compared to stations at other sections of the Manila subduction zone. The plate coupling patterns from the GPS inversion (Fig. 3b) and from a forward model (Fig. 3g) gives similar values of misfit near the subduction of Scarborough Seamount while the distributions of locked patches are fairly different. The results suggest that the fault is likely to be locked with a uniform coupling ratio of about 0.3–0.4 as indicated from GPS inversion (Fig. 3b) or locked at shallow depths (Fig. 3f). If the future seismic rupture occurs on the shallow portion of subduction megathrust as suggested in Fig. 3f, a reassessment of current tsunami hazard is needed in this region. Most previous tsunami models are computed assuming the entire fault rupture along the Manila subduction zone (Liu et al., 2007; Megawati et al., 2009; Wu and Huang, 2009). Additionally, the seismicity offshore western Luzon indicates more frequent earthquakes at latitudes 14.5–16.5°N. Two M ~ 7 earthquakes occurred in 1999 but did not generate significant tsunamis (Figs. 1b and 5).

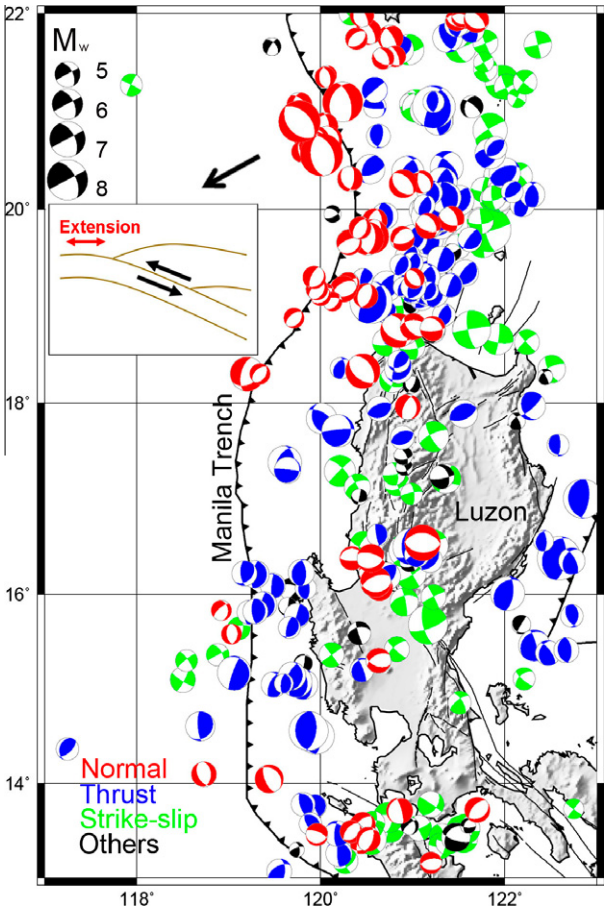

Fig. 5. Earthquake focal mechanisms with depths less than 50 km between 1973 and 2010 from NEIC. Color denotes different fault types shows in bottom left corner. The inset indicates that aseismic subduction causes extension near the outer rise.

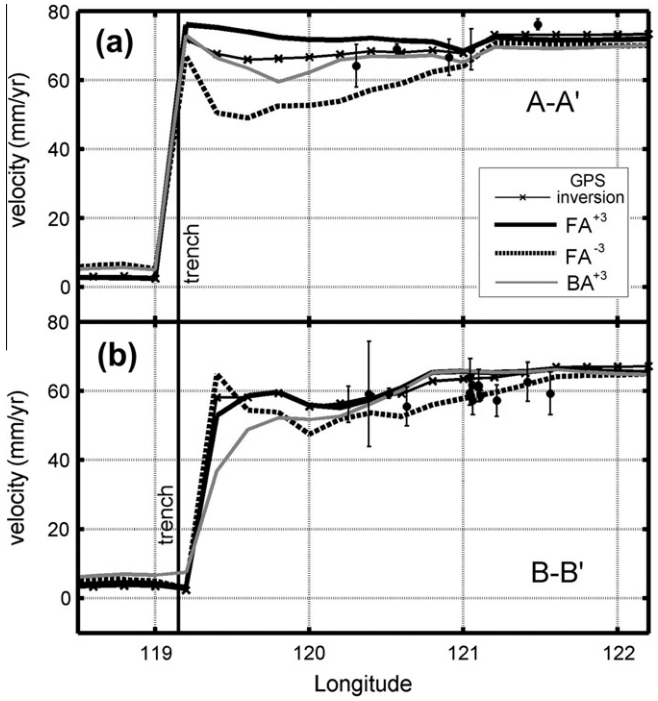

Fig. 6. The east–west cross sections of interseismic velocity predicted by GPS inversion and three TPGA-based plate coupling model at latitude 16.5°N (*A*–*A*′) and 15.5°N (*B*–*B*′). The location of profile is shown in Fig. 3b and the width of the profile is 1°. Vertical line denotes the location of the Manila Trench. Black dots with error bars are observed GPS velocities. The black solid line with cross shows the GPS inversion result. FA^{+3} and FA^{-3} represent the models with coupling ratios proportional and inversely proportional to the cubic of negative free-air TPGA, respectively. BA^{+3} indicate the model with coupling ratio proportional to the cubic of Bouguer TPGA (Table 1).

5. Discussion

Studies have reported that great subduction zone earthquakes are spatially correlated with the locations of forearc basins and gravity lows (Song and Simons, 2003; Wells et al., 2003). While we are not able to obtain reliable relationship between asperities and gravity lows, the preliminary tests offer possible coupling patterns along the Mania Trench based on GPS data and the TPGA maps at other subduction zones. Our results infer a partially locked fault patch extending from the Western Luzon Trough to the northwest coast of Luzon, whereas the fault slip behavior beneath the North Luzon Trough is not well constrained. We find that models with a locked fault patch beneath the North Luzon Trough provides a reasonable fit to GPS data at BTS3 (Fig. 3d and h) and the seismic activity is high at the depth range of 20–50 km near the North Luzon Trough (Fig. 1b). The normal faulting earthquakes are more frequent at the northern part of the Manila subduction zone compared to other sections (Fig. 5). This may suggest that part of accumulated strain is released by aseismic subduction near the North Luzon Trough, thereby causing extension near the outer rise region as indicated in Fig. 5.

Our model infers that plate interface is partially locked with slip-deficit rate of 20–30 mm/yr, equivalent to a coupling ratio of 0.4, in the region between the West Luzon Trough and the east of the subducted Scarborough Seamount chain. Recent studies have shown that the subduction geomorphology features such as ridges, seamounts (Cloos, 1992), and horst and graben structures (Tanioka et al., 1997) affect the seismogenic behavior and rupture dynamics (Kanamori and Kikuchi, 1993). The studies on seamount subduction suggest that seamounts can act as either asperities (Cloos, 1992; Scholz and Small, 1997; Abercrombie et al., 2001) or barriers (Kodaira et al., 2000) to earthquake ruptures. For instance, Abercrombie et al. (2001) suggests that the 1994 Java tsunami earthquake ruptured the bathymetry high corresponding to the location of subducting seamount. Some studies have shown that seamount could be a seismic barrier as observed in the Nankai subduction zones (Kodaira et al., 2000; Cummins et al., 2002). Our model is not able to distinguish whether inferred partially locked patches at latitudes 15–17°N are on the top of subducted seamounts (asperities) or surrounding the seamounts. We speculate that if future earthquakes occur in this region, the structural complexity is likely to influence the size of earthquake. For instance, Cummins et al. (2002) shows that the two subevents of the 1946 Nankai earthquake is bounded by a tear and a subducting seamount on the Philippine Sea Plate. The seismicity in the Japan Trench shows that subducting seamounts have produced repeating earthquakes of magnitude $M \sim 7$ and the width of the seamount may influence the area of the rupture (Mochizuki et al., 2008). If the Scarborough Seamount acts as a barrier, it may locally increase the normal stress and resist the seismic rupture propagation beneath the Scarborough Seamount. On the other hand, the Scarborough Seamount may act as an asperity for a future earthquake. Given a coupling ratio of 0.4 and the area of 800 km (200 km × 40 km) affected by the seamount, the earthquake magnitude is possibly in the range of 7–8 according to the empirical relationships (Wells and Coppersmith, 1994).

It is possible that shallow earthquakes near the Manila trench at latitude 14.5–16°N may occur as suggested by the coupling models in Fig. 3f and g. Historic records indicate large tsunamis have hit the China coast and western Luzon (Wang and Zhang, 2005; Megawati et al., 2009). The investigation of recent shallow subduction zone earthquakes finds that the regions wherein ocean floor is highly faulted near the trench are more likely to produce shallow earthquakes. In addition, the ocean survey shows that the seafloor near the Scarborough Seamount is highly fractured and the trench is filled with sediments (Hayes and Lewis, 1984; Pautot and Rangin, 1989). Seismic rupture propagates in sediments at shallow depths will not only make the earthquake source slow but also cause great seafloor deformation and increase tsunami potential (Polet and Kanamori, 2000).

Early work on tsunami scenarios resulting from earthquakes along the Manila Trench assume that the rupture break the whole plate interface from 13°N to 21°N (Liu et al., 2007; Megawati et al., 2009; Wu and Huang, 2009). Our model infers that fault patches extending from the West Luzon Trough to the east of Scarborough Seamount chain is possibly aseismic. We also speculate that the seafloor roughness associated with the Scarborough Seamount is likely to disrupt the megathrust rupture along the Manila Trench. Our study provides different rupture models from previous rupture scenarios used in tsunami hazards (Liu et al., 2007; Megawati et al., 2009; Wu and Huang, 2009). To better assess the seismic hazard in the South China Sea region, a new generation of tsunami simulations along the Manila Trench is required.

Limited by geographically configuration and insufficient instrumentation, the seismogenic behaviors offshore northern Luzon remain poorly constrained. The region near the Zambales Range is the most closest to the trench axis at the Manila subduction zone. If more GPS sites can be installed in this area (14–16°N), we may be able to investigate the role of the Scarborough Seamount in the seismogenic behavior of the Manila subduction zone and evaluate various plate coupling patterns at this section. Assuming that TPGA-based plate coupling model is a good approximation for future earthquake ruptures, we can compute interseismic GPS velocities from these models. Fig. 6 shows predicted GPS velocities from three TPGA-based coupling models (Fig. 3d–f) along two east–west profiles at latitudes 16.5°N (A–A') and 15.5°N (B–B'). The model with strong coupling corresponding to the cubic of negative Bouguer TPGA gives the smallest misfit in A–A' (Fig. 6a). The fits to the GPS velocities at B–B' are similar for three TPGA-based plate coupling model (Figs. 3d–f and 6b). In order to distinguish these models and explore other possible rupture scenarios in this region, we will densify GPS network in central Luzon. This study shows that the detailed plate coupling pattern is not able to obtain without geodetic observations close to the Manila Trench (Fig. 6). Recent studies of the 2011 M_w9.0 Tohoku–Oki, Japan earthquake and several offshore subduction earthquakes have demonstrated the importance of seafloor geodetic observations to assess the spatial relationship between interseismic coupling and coseismic slip as well as fault rupture behaviors (Baba et al., 2006; Fujita et al., 2006; Matsumoto et al., 2008; Sato et al., 2011a,b). The seafloor geodetic data is substantial to investigate seismogenic behaviors close to the trench.

6. Conclusion

Our model infers that the plate interface between the Manila Trench and the western Luzon is predominately aseismic. The high slip-deficit rate of about 20–30 mm/yr, equivalent to a coupling ratio of 0.4, is found from the West Luzon Trough to the east of the Scarborough Seamount. The seafloor roughness and subducted sediments may complicate the seismogenic behavior at this section such that the entire rupture along the Manila trench seems to be unlikely. We examine a variety of plate coupling patterns based on GPS data, free-air and Bouguer TPGA, as well as forward models. Although we cannot find conclusive relationship between locked fault patches and gravity lows, these alternative coupling models provide plausible rupture scenarios which are not constrained by GPS data. To further explore the role of subducted Scarborough Seamount in seismogenic behavior along the west Luzon coast

and examine plate coupling patterns in details, the densification of GPS network and the seafloor geodesy are required.

Acknowledgements

The authors thank Mark Simons for helpful discussions and many colleagues at the Philippine Institute of Volcanology and Seismology and the Institute of Earth Sciences, Academia Sinica who participated in Luzon GPS surveys. We also thank Ministry of the Interior (MOI) of Taiwan and International GNSS Service (IGS) community for providing the continuous GPS data in this study. Many figures in this paper were generated using the generic mapping tools (GMT) (Wessel and Smith, 1998). This study was financially supported by Academia Sinica and National Science Council of Taiwan under grant NSC 100-2116-M-001-017. This is a contribution of the Institute of Earth Sciences, Academia Sinica, IESAS1639.

References

Abercrombie, R.E., Antolik, M., Felzer, K., Ekstrom, G., 2001. The 1994 Java tsunami earthquake: slip over a subducting seamount. Journal of Geophysical Research 106, 6595–6607.

Altamimi, Z., Collilieux, X., Legrand, J., Garayt, B., Boucher, C., 2007. ITRF2005: a new release of the International Terrestrial Reference Frame based on time series of station positions and earth orientation parameters. Journal of Geophysical Research 112. doi:10.1029/2007JB004949.

Aurelio, M.A., 2000. Shear partitioning in the Philippines: constraints from Philippine Fault and global positioning system data. Island Arc 9, 584–597.

Baba, T., Hirata, K., Hori, T., Sakaguchi, H., 2006. Offshore geodetic data conducive to the estimation of the afterslip distribution following the 2003 Tokachi-oki earthquake. Earth and Planetary Science Letters 241, 281–292.

Bacolcol, T., Aguilar, A., Jorgio, G., de la Cruz, R., Lasala, M., 2005. GPS constraints on the Philippine Fault slip rate in Masbate Island, Central Philippines. Journal of the Geological Society of Philippines 60.

Barrier, E., Huchon, P., Aurelio, M., 1991. Philippine fault – a key for Philippine kinematics. Geology 19, 32–35.

Bautista, B.C., Bautista, M.L.P., Oike, K., Wu, F.T., Punongbayan, R.S., 2001. A new insight on the geometry of subducting slabs in northern Luzon, Philippines. Tectonophysics 339, 279–310.

Bilek, S.L., Schwartz, S.Y., DeShon, H.R., 2003. Control of seafloor roughness on earthquake rupture behavior. Geology 31, 455–458.

Bilham, R., Engdahl, R., Feldl, N., Satyabala, S.P., 2005. Partial and complete rupture of the Indo-Andaman plate boundary 1847–2004. Seismological Research Letters 76, 299–311.

Bowin, C., Lu, R.S., Lee, C.S., Schouten, H., 1978. Plate convergence and accretion in Taiwan–Luzon region. American Association of Petroleum Geologists Bulletin 62, 1645–1672.

Chamot-Rrooke, N., Le Pichon, X., 1999. GPS determined eastward Sundaland motion with respect to Eurasia confirmed by earthquakes slip vectors at Sunda and Philippine trenches. Earth and Planetary Science Letters 173, 439–455.

Chlieh, M., Avouac, J.P., Hjorleifsdottir, V., Song, T.R.A., Ji, C., Sieh, K., Sladen, A., Hebert, H., Prawirodirdjo, L., Bock, Y., Galetzka, J., 2007. Coseismic slip and afterslip of the great M-w 9.15 Sumatra–Andaman earthquake of 2004. Bulletin of the Seismological Society of America 97, S152–S173.

Cloos, M., 1992. Thrust-type subduction-zone earthquakes and seamount asperities – a physical model for seismic rutpure. Geology 20, 601–604.

Cummins, P.R., Baba, T., Kodaira, S., Kaneda, Y., 2002. The 1946 Nankai earthquake and segmentation of the Nankai Trough. Physics of the Earth and Planetary Interiors 132, 75–87.

Fujita, M., Ishikawa, T., Mochizuki, M., Sato, M., Toyama, S., Katayama, M., Kawai, K., Matsumoto, Y., Yabuki, T., Asada, A., Colombo, O.L., 2006. GPS/acoustic seafloor geodetic observation: method of data analysis and its application. Earth Planets and Space 58, 265–275.

Harris, R.A., Segall, P., 1987. Detection of a locked zone at depth on the Parkfield, California, segment of the San-andreas Fault. Journal of Geophysical Research 92, 7945–7962.

Hayes, D.E., Lewis, S.D., 1984. A geophysical-study of the Manila Trench, Luzon, Philippines. 1. Crustal structure, gravity, and regional tectonic evolution. Journal of Geophysical Research 89, 9171–9195.

Herring, T.A., King, R.W., McClusky, S.C., 2002. Documentation for the GAMIT Analysis Software, release 10.0 edn. Massachusetts Institute of Technology, Cambridge, MA, p. 183.

Hyndman, R.D., Yamano, M., Oleskevich, D.A., 1997. The seismogenic zone of subduction thrust faults. Island Arc 6, 244–260.

Kanamori, H., 1986. Rupture process of subduction zone earthquakes. Annual Review of Earth and Planetary Sciences 14, 293–322.

Kanamori, H., Kikuchi, M., 1993. The 1992 Nicaraguaearthquake – a slow tsunami earthquake associated with subducted sediments. Nature 361, 714–716.

Karig, D.E., 1983. Accreted terranes in the northern part of the Philippine archipelago. Tectonics 2, 211–236.

Kodaira, S., Takahashi, N., Nakanishi, A., Miura, S., Kaneda, Y., 2000. Subducted seamount imaged in the rupture zone of the 1946 Nankaido earthquake. Science 289, 104–106.

Kreemer, C., Holt, W.E., Goes, S., Govers, R., 2000. Active deformation in eastern Indonesia and the Philippines from GPS and seismicity data. Journal of Geophysical Research 105, 663–680.

Kreemer, C., Holt, W.E., Haines, A.J., 2003. An integrated global model of present-day plate motions and plate boundary deformation. Geophysical Journal International 154, 8–34.

Lewis, S.D., Hayes, D.E., 1984. A geophysical study of the Manila Trench, Luzon, Philippines. 2. Fore arc basin structural and stratigraphic evolution. Journal of Geophysical Research 89, 9196–9214.

Liu, Y.C., SantoS, A., Wang, S.M., Shi, Y.L., Liu, H.L., Yuen, D.A., 2007. Tsunami hazards along Chinese coast from potential earthquakes in South China Sea. Physics of the Earth and Planetary Interiors 163, 233–244.

Llenos, A.L., McGuire, J.J., 2007. Influence of fore-arc structure on the extent of great subduction zone earthquakes. Journal of Geophysical Research 112. doi:10.1029/2007JB004944.

Ludwig, W.J., 1970. The Manila trench and West Luzon Trough – III. Seismic-refraction measurements. Deep-Sea Research 17, 553–571.

Ludwig, W.J., Kumar, N., Houtz, R.E., 1979. Profiler-sonobuoy measurements in the South Chian Sea basin. Journal of Geophysical Research 84, 3505–3518.

Matsumoto, Y., Ishikawa, T., Fujita, M., Sato, M., Saito, H., Mochizuki, M., Yabuki, T., Asada, A., 2008. Weak interplate coupling beneath the subduction zone off Fukushima, NE Japan, inferred from GPS/acoustic seafloor geodetic observation. Earth Planets and Space 60, E9–E12.

Matthews, M.V., Segall, P., 1993. Estimation of depth-dependent fault slip from measured surface deformation with application to the 1906 San-Francisco earthquake. Journal of Geophysical Research 98, 12153–12163.

Megawati, K., Shaw, F., Sieh, K., Huang, Z.H., Wu, T.R., Lin, Y.N., Tan, S.K., Pan, T.C., 2009. Tsunami hazard from the subduction megathrust of the South China Sea: Part I. Source characterization and the resulting tsunami. Journal of Asian Earth Sciences 36, 13–20.

Mochizuki, K., Yamada, T., Shinohara, M., Yamanaka, Y., Kanazawa, T., 2008. Weak interplate coupling by seamounts and repeating M similar to 7 earthquakes. Science 321, 1194–1197.

Okada, Y., 1985. Surface deformation to shear and tensile faults in a half space. Bulletin of the Seismological Society of America 75, 1135–1154.

Ortiz, M., Bilham, R., 2003. Source area and rupture parameters of the 31 December 1881 M-w = 7.9 Car Nicobar earthquake estimated from tsunamis recorded in the Bay of Bengal. Journal of Geophysical Research 108. doi:10.1029/2002JB001941.

Pacheco, J.F., Sykes, L.R., Scholz, C.H., 1993. Nature of seismic coupling along simple plate boundaries of the subduction type. Journal of Geophysical Research 98, 14133–14159.

Page, B.M., Suppe, J., 1981. The Pliocene Lichi melange of Taiwan: its plate tetonic and olistostromal origin. American Journal of Sciences 281, 193–227.

Pautot, G., Rangin, C., 1989. Subduction of the South China Sea axial ridge below Luzon (Philippines). Earth and Planetary Science Letters 92, 57–69.

Peacock, S.M., Hyndman, R.D., 1999. Hydrous minerals in the mantle wedge and the maximum depth of subdcution thrust earthquakes. Geophysical Research Letters 26, 2517–2520.

Polet, J., Kanamori, H., 2000. Shallow subduction zone earthquakes and their tsunamigenic potential. Geophysical Journal International 142, 684–702.

Rangin, C., Le Pichon, X., Mazzotti, S., Pubellier, M., Chamotrooke, N., Aurelio, M., Walpersdorf, A., Quebral, R., 1999. Plate convergence measured by GPS across the Sundaland/Philippine sea plate deformed boundary: the Philippines and eastern Indonesia. Geophysical Journal International 139, 296–316.

Ruff, L.J., 1989. Do trench sediments affect great earthquake occurence in subduction zones. Pure and Applied Geophysics 129, 263–282.

Ruff, L., Kanamori, H., 1980. Seismicity and the subduction process. Physics of the Earth and Planetary Interiors 23, 240–252.

Sandwell, D.T., Smith, W.H.F., 2009. Global marine gravity from retracked Geosat and ERS-1 altimetry: Ridge segmentation versus spreading rate. Journal of Geophysical Research 114. doi:10.1029/2008JB006008.

Sato, M., Ishikawa, T., Ujihara, N., Yoshida, S., Fujita, M., Mochizuki, M., Asada, A., 2011a. Displacement above the hypocenter of the 2011 Tohoku–Oki earthquake. Science 332, 1395.

Sato, M., Saito, H., Ishikawa, T., Matsumoto, Y., Fujita, M., Mochizuki, M., Asada, A., 2011b. Restoration of interplate locking after the 2005 Off-Miyagi Prefecture earthquake, detected by GPS/acoustic seafloor geodetic observation. Geophysical Research Letters 38. doi:10.1029/2010gl045689.

Savage, J.C., 1983. A dislocation model of strain accumulation and release at a subduction zone. Journal of Geophysical Research-Solid Earth 88, 4984–4996.

Scholz, C.H., Small, C., 1997. The effect of seamount subduction on seismic coupling. Geology 25, 487–490.

Sella, G.F., Dixon, T.H., Mao, A.L., 2002. REVEL: a model for recent plate velocities from space geodesy. Journal of Geophysical Research 107. doi:10.1029/2000JB000033.

Seno, T., Stein, S., Gripp, A.E., 1993. A model for the motion of the Philippine Sea Plate consistent with NUVEL-1 and geological data. Journal of Geophysical Research 98, 17941–17948.

Simons, W.J.F., Ambrosius, B.A.C., Noomen, R, Angermann, D., Wilson, P., Becker, M., Reinhart, E., Walpersdorf, A., Vigny, C., 1999. Observing Plate Motions in S.E.

Asia: Geodetic Results of the GEODYSSEA Project, edn, American Geophysical Union, Washington, DC, ETATS-UNIS.

Song, T.R.A., Simons, M., 2003. Large trench-parallel gravity variations predict seismogenic behavior in subduction zones. Science 301, 630–633.

Stern, R.J., 2002. Subduction zones. Reviews of Geophysics 40. doi:10.1029/2001rg000108.

Tanioka, Y., Ruff, L., Satake, K., 1997. What controls the lateral variation of large earthquake occurrence along the Japan Trench? Island Arc 6, 261–266.

Uyeda, S., Kanamori, H., 1979. Back-arc opening and the mode of subduction. Journal of Geophysical Research 84, 1049–1061.

Wang, F., Zhang, Z.Q., 2005. Earthquake tsunami record in Chinese ancient books. China Earthquakes 21, 9.

Wells, D.L., Coppersmith, K.J., 1994. New empirical relationships among magnitude, rupture length, rupture width, rupture area, and surface displacement. Bulletin of the Seismological Society of America 84, 974–1002.

Wells, R.E., Blakely, R.J., Sugiyama, Y., Scholl, D.W., Dinterman, P.A., 2003. Basin-centered asperities in great subduction zone earthquakes: a link between slip, subsidence, and subduction erosion? Journal of Geophysical Research 108. doi:10.1029/2002JB002072.

Wu, T.R., Huang, H.C., 2009. Modeling tsunami hazards from Manila trench to Taiwan. Journal of Asian Earth Sciences 36, 21–28.

Yu, S.B., Kuo, L.C., Punongbayan, R.S., Ramos, E.G., 1999. GPS observation of crustal deformation in the Taiwan–Luzon region. Geophysical Research Letters 26, 923–926.

Yu, S.B., Hsu, Y.J., Bacolcol, T., Yang, C.C., Tsai, Y.C., Solidum, R., 2011. Present-day crustal deformation along the Philippine fault in Luzon, Philippines. Journal of Asian Earth Sciences. doi:10.1016/j.jseaes.2010.12.007.